

## Facile synthesis of composite polyferric magnesium–silicate–sulfate coagulant with enhanced performance in water and wastewater

Xiangtao Huo, Rongxia Chai, Lizheng Gou, Mei Zhang, and Min Guo

Cite this article as:

Xiangtao Huo, Rongxia Chai, Lizheng Gou, Mei Zhang, and Min Guo, Facile synthesis of composite polyferric magnesium–silicate–sulfate coagulant with enhanced performance in water and wastewater, *Int. J. Miner. Metall. Mater.*, 31(2024), No. 3, pp. 574-584. <https://doi.org/10.1007/s12613-023-2704-8>

View the article online at [SpringerLink](#) or [IJMMM Webpage](#).

### Articles you may be interested in

Yang Hu, Chun-bao Sun, and Jue Kou, [Exfoliation of poly\(ethylene glycol\)-intercalated graphite oxide composite in water without sonication](#), *Int. J. Miner. Metall. Mater.*, 27(2020), No. 6, pp. 840-845. <https://doi.org/10.1007/s12613-019-1932-4>

Ping-chao Ke, Zhi-hong Liu, and Lin Li, [Synthesis, characterization, and property test of crystalline polyferric sulfate adsorbent used in treatment of contaminated water with a high As\(III\) content](#), *Int. J. Miner. Metall. Mater.*, 25(2018), No. 10, pp. 1217-1225. <https://doi.org/10.1007/s12613-018-1674-8>

Youness Rakhila, Abdellah Elmchaouri, Allal Mestari, Sophia Korili, Meriem Abouri, and Antonio Gil, [Adsorption recovery of Ag\(I\) and Au\(III\) from an electronics industry wastewater on a clay mineral composite](#), *Int. J. Miner. Metall. Mater.*, 26(2019), No. 6, pp. 673-680. <https://doi.org/10.1007/s12613-019-1777-x>

Fabiane Carvalho Ballotin, Mayra Nascimento, Sara Silveira Vieira, Alexandre Carvalho Bertoli, Ottávio Carmignano, Ana Paula de Carvalho Teixeira, and Rochel Montero Lago, [Natural Mg silicates with different structures and morphologies: Reaction with K to produce  \$K\_2MgSiO\_4\$  catalyst for biodiesel production](#), *Int. J. Miner. Metall. Mater.*, 27(2020), No. 1, pp. 46-54. <https://doi.org/10.1007/s12613-019-1891-9>

He-fei Zhao, Hong-ying Yang, Lin-lin Tong, Qin Zhang, and Ye Kong, [Biooxidationthiosulfate leaching of refractory gold concentrate](#), *Int. J. Miner. Metall. Mater.*, 27(2020), No. 8, pp. 1075-1082. <https://doi.org/10.1007/s12613-020-1964-9>

Meng-ting Duan, Meng-rong Wu, Kai Xue, Zheng-xu Bian, Jing Shi, Xing-mei Guo, Fu Cao, Jun-hao Zhang, Qing-hong Kong, and Feng Zhang, [Preparation of  \$CoO/SnO\_2@NC/S\$  composite as high-stability cathode material for lithium-sulfur batteries](#), *Int. J. Miner. Metall. Mater.*, 28(2021), No. 10, pp. 1647-1655. <https://doi.org/10.1007/s12613-021-2315-1>



IJMMM WeChat



QQ author group

# Facile synthesis of composite polyferric magnesium–silicate–sulfate coagulant with enhanced performance in water and wastewater

Xiangtao Huo, Rongxia Chai, Lizheng Gou, Mei Zhang, and Min Guo✉

School of Metallurgical and Ecological Engineering, University of Science and Technology Beijing, Beijing 100083, China

(Received: 15 February 2023; revised: 7 July 2023; accepted: 10 July 2023)

**Abstract:** The coagulation process is a widely applied technology in water and wastewater treatment. Novel composite polyferric magnesium–silicate–sulfate (PFMS) coagulants were synthesized using  $\text{Na}_2\text{SiO}_3 \cdot 9\text{H}_2\text{O}$ ,  $\text{Fe}_2(\text{SO}_4)_3$ , and  $\text{MgSO}_4$  as raw materials in this paper. The effects of aging time, Fe:Si:Mg, and OH:M molar ratios (M represents the metal ions) on the coagulation performance of the as-prepared PFMS were systematically investigated to obtain optimum coagulants. The results showed that PFMS coagulant exhibited good coagulation properties in the treatment of simulated humic acid–kaolin surface water and reactive dye wastewater. When the molar ratio was controlled at Fe:Si:Mg = 2:2:1 and OH:M = 0.32, the obtained PFMS presented excellent stability and a high coagulation efficiency. The removal efficiency of ultraviolet  $\text{UV}_{254}$  was 99.81%, and the residual turbidity of the surface water reached 0.56 NTU at a dosage of 30  $\text{mg} \cdot \text{L}^{-1}$ . After standing the coagulant for 120 d in the laboratory, the removal efficiency of  $\text{UV}_{254}$  and residual turbidity of the surface water were 88.12% and 0.68 NTU, respectively, which accord with the surface water treatment requirements. In addition, the coagulation performance in the treatment of reactive dye wastewater was greatly improved by combining the advantages of magnesium and iron salts. Compared with polyferric silicate–sulfate (PFS) and polymagnesium silicate–sulfate (PMS), the PFMS coagulant played a better decolorization role within the pH range of 7–13.

**Keywords:** polyferric–magnesium–silicate–sulfate; composite coagulants; water and wastewater; excellent stability; high coagulation efficiency; decolorization

## 1. Introduction

Coagulation process, an important part of water treatment, has been widely used in water supply and wastewater treatment for the removal of colloidal particles and dissolved organics [1–6]. The quality of the above process directly affects the effect and cost of subsequent treatment of wastewater. With increasingly serious environmental pollution and strict water quality standards [7–8], conventional coagulation technology fails to meet the demands for water quality and safety. Therefore, the development of novel and efficient flocculants has consistently been a key research object in the field of water treatment and environmental protection [9–10].

Traditional coagulants including  $\text{Al}_2(\text{SO}_4)_3$  [11],  $\text{Fe}_2(\text{SO}_4)_3$  [12],  $\text{AlCl}_3$  [13], and  $\text{FeCl}_3$  [14] can hydrolyze rapidly and form high-charge intermediate products, such as  $\text{Al}_2(\text{OH})_2^{4+}$ ,  $\text{Al}_3(\text{OH})_4^{5+}$ ,  $\text{Fe}_2(\text{OH})_2^{4+}$ , and  $\text{Fe}_3(\text{OH})_5^{5+}$ . However, the coagulants are easy to destabilize colloids by adsorbing on the surfaces. Iron salt flocculants are highly corrosive to the equipment during the treatment process, and residual  $\text{Fe}^{3+}$  ions are usually darker compared with other ions. Meanwhile, the applications of aluminum salt flocculants are limited due to the toxicity of aluminum ions [15]. Given the synergistic effects of hybrid compositions, scholars have conducted

a number of studies on the combination of metal-based complex cationic materials with anionic groups (including  $\text{Na}_2\text{SiO}_3$ ,  $\text{NaH}_2\text{PO}_4$ ,  $\text{H}_3\text{PO}_4$ , etc) [16–19]. The low-molecular-weight metal salt flocculants are gradually being replaced by inorganic polymer flocculants, which mainly contain aluminum- and iron-based inorganic polymer flocculants, polysilicate flocculants, and magnesium salt flocculants [20–26]. For instance, Tolkou *et al.* [27] combined polyaluminum chloride with ferric species and polysilicic acid (PS) to prepare composite polyaluminum–ferric silicate–chloride coagulants using two polymerization techniques, namely, the copolymerization process and composite polymerization method. The former is more effective than the latter. Specifically, composite polymerization and copolymerization are conventional methods for the preparation of polysilicate complex coagulants. The former involves the polymerization of PS and hydroxylated metal salts, and the latter refers to the hydroxylation of mixture of metal salts and PS [28]. The coagulants are essential for the hydroxylation of Si and metal ions, and the structures and coagulation performances can be influenced by preparation methods. For instance, the polyferric aluminum–silica–sulfate coagulant prepared by composite polymerization showed better performances in the removal of turbidity, COD, and chroma than polyaluminum chloride

✉ Corresponding author: Min Guo E-mail: [guomin@ustb.edu.cn](mailto:guomin@ustb.edu.cn)

© University of Science and Technology Beijing 2024

[29]. In a study on the reaction mode between Si and Fe in polysilicic ferric (PSF) coagulant prepared by copolymerization, PSF contained some complex compounds, and its characteristics were largely affected by the reaction time and Si/Fe ratio [30]. The polyferric silicate–chloride synthesized by copolymerization showed three- and two-dimensional growth of Fe species at low and high Si/Fe ratios, respectively [31]. The polyferric silicate sulfate coagulants prepared by copolymerization had a higher coagulation efficiency than those prepared by composite polymerization [28]. Therefore, the preparation of polysilicate complex coagulants by copolymerization has been the more popular option [32–34]. Chen *et al.* [35] conducted a detailed study on the characterization and coagulation performance of polyferric aluminum–silicate–sulfate. The results indicated that the adsorption/bridge formation mechanism was predominant at a low coagulant dosage, and adsorption/charge neutralization became more important under high coagulant dosages. Although widespread attention has been paid to Al–Fe composite coagulants, other novel coagulants have been developed due to the potential side effects of aluminum salts on human health [33,36–39]. Zhu *et al.* [40] created a polymeric zinc–iron–phosphate coagulant by introducing zinc and  $\text{PO}_4^{3-}$  to an iron solution. The prepared coagulant effectively removed the dissolved organic nitrogen, which can be characterized by a dense convex–concave packing structure. Wei *et al.* [38] prepared a polysilicate–magnesium using different acids as media. The polysilicate–magnesium–sulfate presented a compact gel network structure with an efficient coagulation performance in dyeing wastewater treatment. In addition, the removal of impurities or pollutants can be enhanced in the presence of magnesium salt [41–42]. Moreover, magnesium can neutralize the remaining color of iron salt and broaden the pH range of coagulants simultaneously, as magnesium is more effective at high pH [43–44]. Meanwhile, a few studies reported the preparation of polyferric–magnesium–silicate–sulfate (PFMS) coagulant, and many problems remain to be solved.

This work was designed to investigate the synthesis, characterization, and coagulation properties of PFMS to fill the gap in the literature. Given that the research on the preparation of PFMS coagulant is in its infancy, PFMS deserves research attention due to the synergetic effect of this component in a single material. The effects of aging time, molar ratio of Fe, Si, and Mg (Fe:Si:Mg), and molar ratio of OH and M (OH:M) (M represents the metal ions) on the structure and coagulation properties of the as-prepared PFMS were systematically investigated to obtain an optimized preparation condition. In addition, the coagulation efficiency of PFMS coagulants was evaluated in the treatment of simulated humic acid–kaolin suspension and reactive dye wastewater. Compared with polyferric silicate–sulfate (PFS) and polymagnesium silicate–sulfate (PMS), the coagulation mechanism of PFMS was analyzed, which enriched the basic theory of inorganic composite coagulant application.

## 2. Experimental

### 2.1. Materials

$\text{Na}_2\text{SiO}_3 \cdot 9\text{H}_2\text{O}$ ,  $\text{MgSO}_4 \cdot 7\text{H}_2\text{O}$ , and  $\text{Fe}_2(\text{SO}_4)_3 \cdot \text{H}_2\text{O}$  were purchased from the Sinopharm Chemical Reagent Co., Ltd. Humic acid (FA  $\geq 90\%$ ) and kaolin (CP) came from Shanghai Aladdin Biochemical Technology Co., Ltd.  $\text{H}_2\text{SO}_4$  (98%), and NaOH were provided by Beijing Chemical Factory.

### 2.2. Preparation of the PFMS coagulant

PFMS was prepared via a copolymerization approach [45–46] (Fig. 1). First,  $0.40 \text{ mol} \cdot \text{L}^{-1}$  (as Si)  $\text{Na}_2\text{SiO}_3 \cdot 9\text{H}_2\text{O}$  solution was dripped slowly into  $2.32 \text{ mol} \cdot \text{L}^{-1}$   $\text{H}_2\text{SO}_4$  solution at a stirring rate of  $200 \text{ r} \cdot \text{min}^{-1}$  under an ambient condition. Subsequently,  $1.0 \text{ mol} \cdot \text{L}^{-1}$  NaOH was added to the above solution and mixed under magnetic agitation for 1.5 h to adjust the pH to 2.0. The PS solution was obtained [38]. Second, based on the predetermined Fe:Si:Mg, certain amounts of  $\text{Fe}_2(\text{SO}_4)_3$  ( $0.26 \text{ mol} \cdot \text{L}^{-1}$ ) and  $\text{MgSO}_4$  ( $0.10 \text{ mol} \cdot \text{L}^{-1}$ ) solution were added to the newly prepared PS under magnetic stirring. Then,  $1.0 \text{ mol} \cdot \text{L}^{-1}$   $\text{NaHCO}_3$  solution was slowly added to the mixed solution to achieve the predetermined OH:M, and the stirring speed was increased to  $280 \text{ r} \cdot \text{min}^{-1}$  to avoid precipitation. Finally, the formed PFMS solution was stirred at  $200 \text{ r} \cdot \text{min}^{-1}$  for 3 h and then aged for 3 d to complete the preparation process. In addition, PFS was obtained through adding diluted iron sulfate to fresh polysilicate solution at molar ratio of Fe:Si = 1:1, and the molar ratio of OH and Fe ( $r_{\text{OH:Fe}}$ ) was adjusted to 0.32 using a sodium bicarbonate solution. The PMS was obtained via the addition of diluted magnesium sulfate to the fresh polysilicate solution at molar ratio of Mg:Si = 2:1, and the  $r_{\text{OH:Fe}}$  was adjusted to 0.32 by a sodium bicarbonate solution.

### 2.3. Characterization of PFMS coagulant

The liquid PFMS was dried in a drying oven at  $50^\circ\text{C}$  to

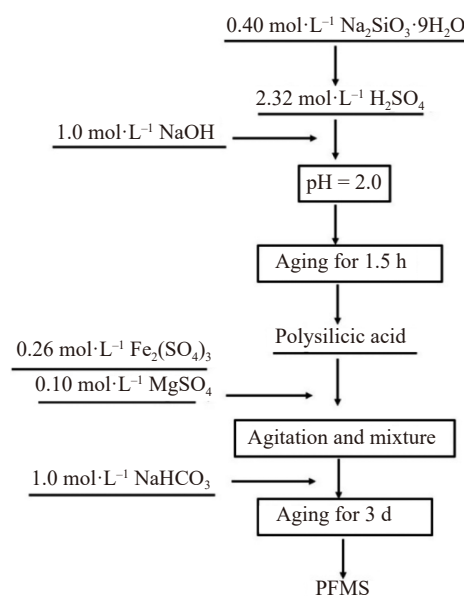


Fig. 1. Flow chart of PFMS coagulant synthesis process.

obtain the ground powder, and X-ray diffraction (XRD, TTR3, Rigaku, Japan), Fourier transform infrared spectrometer (FT-IR, Avater360, Nicolet, USA), and scanning electron microscope (SEM, Supra-55, Zeiss, Germany) were used to characterize the structure and morphology of the coagulants. The particle size and zeta ( $\zeta$ ) potential measurements were analyzed using a Zetasizer Nano ZS90 analyzer (Malvern). The particle size (volume distribution) of broken flocs was determined by an LMS-30 size distribution analyzer. The concentration of metal ions in the solution was detected by inductively coupled plasma atomic emission spectroscopy (ICP-OES, OPTIMA 7000DV, America).

2.4. Coagulation experiments

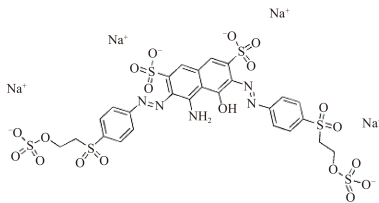
In our experiment, a six-paddle jar tester (HJ-6B, China)

with six cylinders (100 mL) was used to visualize the deposition behavior of the samples. Two water samples were treated: (1) a typical humic acid–kaolin synthetic surface water containing 50 mg·L<sup>-1</sup> kaolin and 10 mg·L<sup>-1</sup> humic acid and (2) reactive dye wastewater with 50 mg·L<sup>-1</sup> reactive black dye. Tables 1 and 2 summarize the general water quality of the raw water. First, each cylinder was filled with 50 mL of model wastewater. After the addition of different dosages of coagulants, the suspension was rapidly mixed at 220 r·min<sup>-1</sup> for 2 min to achieve uniform dispersion. At this point, 10 mL samples were removed to measure the zeta ( $\zeta$ ) potential. Subsequently, the suspension was stirred slowly at 60 r·min<sup>-1</sup> for 6 min and then placed for 10 min to sink the precipitation.

Table 1. Typical properties of humic acid–kaolin synthetic surface water

pH	Turbidity / NTU	Zeta potential / mV	Absorbance at UV <sub>254</sub>
7.8–7.95	58–60	–20.5––20.2	0.084–0.086

Table 2. Reactive black dye characterization

Type	Molecular structure	$\lambda_{\text{max, dye}} / \text{nm}$
Azo		616

A supernatant sample (2.0 cm below the surface) was collected to measure the residual turbidity with a 2100Q Turbimeter (HACH, America). Meanwhile, the surface water was filtered through a 0.45  $\mu\text{m}$  filter to measure the UV<sub>254</sub> with a TU-1901 spectrophotometer. The UV<sub>254</sub> removal efficiency was calculated using Eq. (1):

$$\text{UV}_{254} \text{ removal efficiency} = \frac{A_0 - A}{A_0} \times 100\% \tag{1}$$

where  $A_0$  is the initial absorbance value of the raw water tested at 254 nm, and  $A$  is the absorbance value of samples collected after the coagulation treatment.

In addition, the decoloration removal efficiency was calculated following Eq. (2):

$$\text{Decoloration removal efficiency} = \frac{A' - A}{A'} \times 100\% \tag{2}$$

where  $A'$  is the initial absorbance value of the raw water tested at  $\lambda_{\text{max, dye}}$ .

3. Results and discussion

3.1. Effect of Fe:Si:Mg on the structure and morphology of PFMS

Fig. 2 exhibits the XRD spectra of the as-prepared PFS, PMS, and PFMS samples with different Fe:Si:Mg. The formed PFS and PFMS samples possessed large and broad

peaks at 30°, which indicates an amorphous structure with fuzzy crystal traces. In addition, no characteristic diffraction peaks of Fe<sub>2</sub>(SO<sub>4</sub>)<sub>3</sub>, MgSO<sub>4</sub>, and SiO<sub>2</sub> were observed in the PFMS samples. This characteristic demonstrated that these materials were not mechanically mixed [28,34,46]. Different from PFS and PFMS, the PMS product presented a limited diffraction crystal pattern of SiO<sub>2</sub>. The corresponding valence bond structures were further determined by FT-IR analysis.

Fig. 3 displays the FT-IR spectra of the as-prepared PFS, PMS, and PFMS with different Fe:Si:Mg. All spectra presented absorption peaks at 3500–3340 and 1662–1647 cm<sup>-1</sup>. The former was associated with the intermolecular stretching vibration of –OH, and the latter corresponded to the bending vibration of adsorbed and crystallized water [47]. For PFMS<sub>(6:2:1)</sub>, the intensities of the two peaks were the largest as the high proportion of iron led to a great degree of iron hydrolysis. The adsorption peak of Fe–O–Fe was also observed at 1215 cm<sup>-1</sup> in PFMS<sub>(6:2:1)</sub> and PFMS<sub>(4:2:1)</sub>. However, the peak vanished and was superimposed at approximately 1149–1131

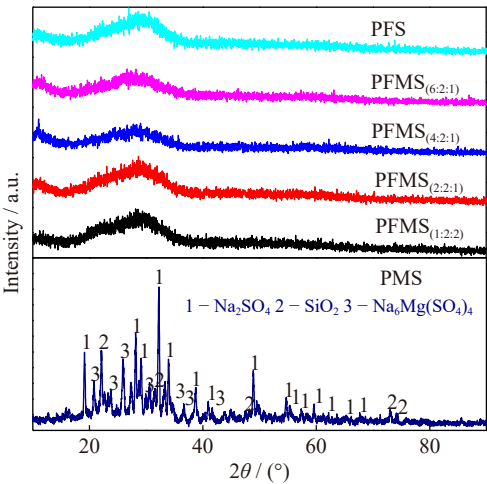


Fig. 2. XRD patterns of the PFS, PMS, and PFMS samples with different Fe:Si:Mg.



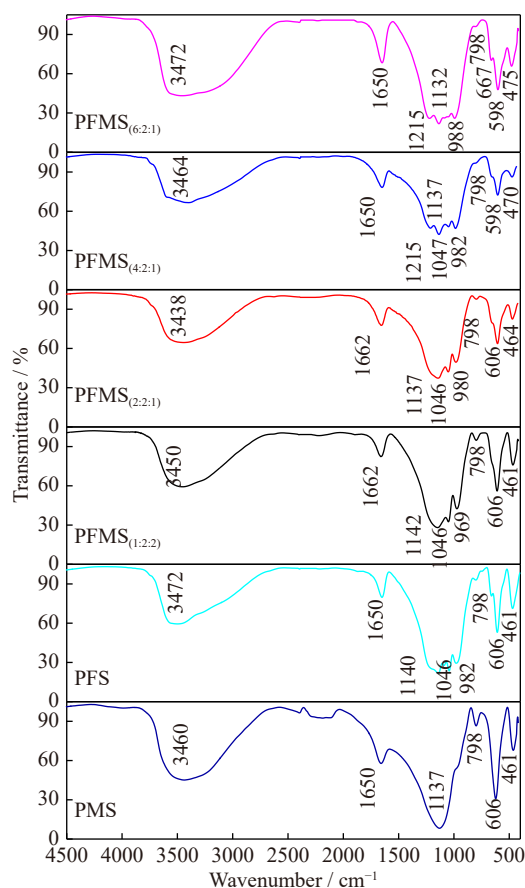


Fig. 3. FT-IR spectra of the PFS, PMS, and PFMS samples with different Fe:Si:Mg.

$\text{cm}^{-1}$ , which was related to the asymmetric Si–O–Si or Fe–O–Fe stretching vibrations [31,48]. Such a phenomenon indicates that the oxygen-bridged polymerization degree increased accordingly and replaced a part of the Fe–O–Fe. The peak at 1053–1046 and 988–969  $\text{cm}^{-1}$  can be assigned to the asymmetric stretching vibration of Fe–O–Fe and stretching vibration of the Fe–O–Si bonds, respectively. In addition, the peak at 798  $\text{cm}^{-1}$  was attributed to the tetrahedron connection of Si–O–Si, and those at 667  $\text{cm}^{-1}$  might have been caused by the bending vibration of Fe–OH. Moreover, two peaks at 606–598 and 475–461  $\text{cm}^{-1}$  corresponded to the bending vibrations of Si–O and Fe–O, respectively [31].

The above results indicated the formation of a polymer with a large network structure, and the bonds observed were further hydrolyzed during the coagulation process, which produced hydroxy complexes of polycore silicon and iron-containing polysilicon portions [46]. These dissolved hydrolyzed polymeric products reacted with colloids to accelerate the colloidal particles and cause their destabilization and coagulation. Furthermore, no new chemical bonds appeared in the PMS coagulant. This phenomenon suggests that  $\text{Mg}^{2+}$  was excluded from the polymerization process. Instead, they were embedded in a large network of iron and silicon by electrostatic forces as free ions, which was consistent with the reported result [49].

The morphological performance of the as-prepared coagulants was an important parameter for their visual analysis.

Fig. 4 shows the SEM images of coagulants PFS, PMS, and PFMS with different Fe:Si:Mg. Fig. 4(a)–(b) shows the clustering units of PFS were long and tree-like and showed three-dimensional, iteratively extending structural features, and PMS displayed irregularly shaped blocks of varying sizes. Compared with the above two coagulants, the surface morphology of PFMS changed remarkably. The PFMS<sub>(6:2:1)</sub> and PFMS<sub>(4:2:1)</sub> presented an evident blocky body structure, as shown in Fig. 4(c)–(d). Furthermore, as the contents of PS and magnesium increased, the PFMS<sub>(1:2:2)</sub> formed a compact gel network structure, which showed a schistose aggregation distribution (Fig. 4(e)). Meanwhile, the PFMS<sub>(2:2:1)</sub> sample revealed the coexistence of a lumpy and flaky structure, and the hydrolysates of the metal salt and PS aggregated to form a product with a large polymerization state (Fig. 4(f)).

### 3.2. Effect of OH:M on the structure and chemical bonds of PFMS

XRD pattern and FT-IR spectra show the effect of the OH:M ratio on the structure and chemical bonds of the as-prepared PFMS, respectively. As displayed in Fig. 5, all samples presented a distinct bulge at  $2\theta = 30^\circ$  regardless of the OH:M, indicating the amorphous structure of all samples. Moreover, as the ratio increased, the high and wide bulges gradually flattened, and the specific complex morphology was further verified through the chemical bond structure. Fig. 6 depicts the FT-IR spectra of PFMS samples prepared with different  $r_{\text{OH:M}}$ . Accordingly, the position of the characteristic absorption peak of the functional groups in the sample was independent of  $r_{\text{OH:M}}$ . However, as the  $r_{\text{OH:M}}$  increased from 0.18 to 0.40, the intensity of the characteristic absorption peak increased substantially, which confirmed the increased polymerization degree of the product and the strong bonding reaction between functional groups. The content of  $\text{OH}^-$  was positively correlated with the polymerization degree of hydroxyl polymers to a certain extent. In addition, the increase in the OH:M led to the hydrolysis and precipitation of iron, which affected the effective composition of the flocculant.

### 3.3. Coagulation performance of PFMS in the treatment of humic acid–kaolin synthetic surface water

#### 3.3.1. Effect of Fe:Si:Mg and dosage of PFMS on the coagulation properties and dominant mechanism in the coagulation process

The chemical structure and morphology of PFMS with different Fe:Si:Mg were analyzed, and the actual coagulation effect of the beaker experiment was used to obtain the optimal ratio of coagulants. Fig. 7(a)–(b) shows the results of the coagulation experiment on the treatment of humic acid–kaolin synthetic surface water based on residual turbidity and removal humic acid rate, respectively. Compared with PFS, PFMS<sub>(4:2:1)</sub> and PFMS<sub>(2:2:1)</sub> exhibited better coagulation performances under a wide coagulation dose. For PFMS<sub>(2:2:1)</sub>, the residual turbidity was 0.56 NTU, and the removal efficiency of  $\text{UV}_{254}$  was 99.81% at a dosage of 30  $\text{mg}\cdot\text{L}^{-1}$ . However, the PFMS<sub>(1:2:2)</sub> was the most ineffective composite coagulant for

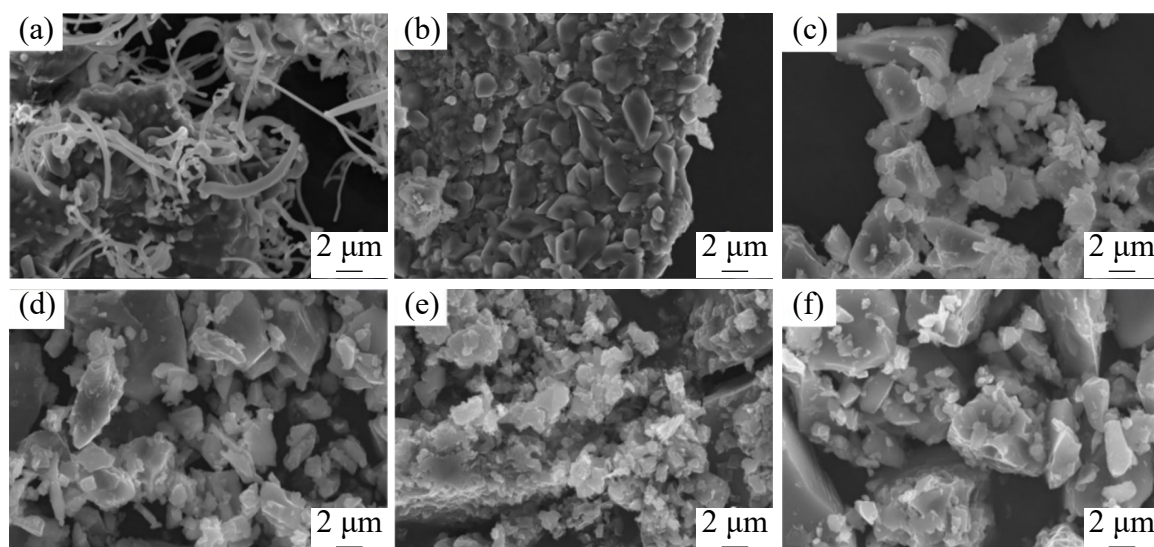


Fig. 4. SEM images of the PFS, PMS, and PFMS samples with different Fe:Si:Mg: (a) PFS; (b) PMS; (c) PFMS<sub>(6:2:1)</sub>; (d) PFMS<sub>(4:2:1)</sub>; (e) PFMS<sub>(1:2:2)</sub>; (f) PFMS<sub>(2:2:1)</sub>.

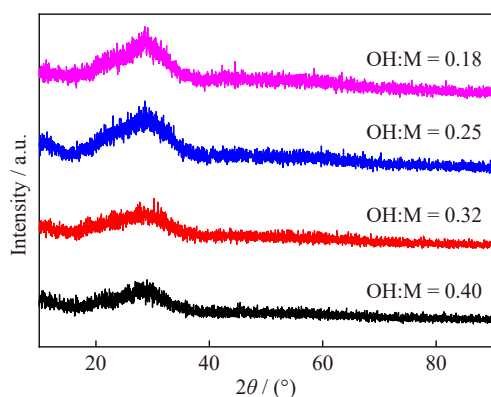


Fig. 5. XRD patterns of PFMS samples with different  $r_{\text{OH:M}}$ .

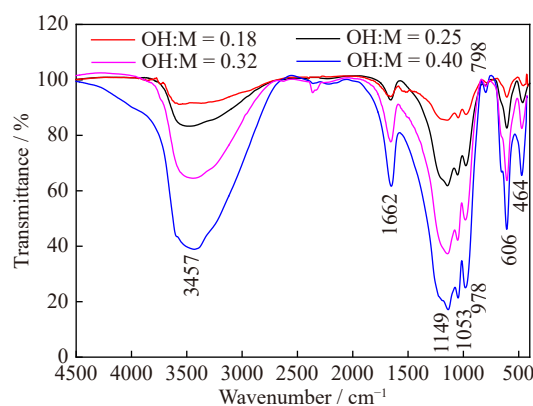


Fig. 6. FT-IR spectra of PFMS samples with different  $r_{\text{OH:M}}$ .

the removal of solid suspensions or organic humic acid. Moreover, as the removal efficiency of PMS for turbidity and humic acid was less than 50%, it was not displayed in the figure. According to the Schulze–Hardy rule, the coagulation capacity can be enhanced when the valence of active counter ions increases [50]. Thus, the main destabilizing effect on colloids depended on  $\text{Fe}^{3+}$  and its hydrolysis product rather than  $\text{Mg}^{2+}$ . However, the iron content should not be extremely high given that the brown precipitate occurred in

PFMS<sub>(6:2:1)</sub> after 25 d.

Moreover, as the amount of coagulant increased from 9 to  $50 \text{ mg} \cdot \text{L}^{-1}$ , the zeta potential of colloidal particles increased from  $-12$  to  $-2 \text{ mV}$ , which demonstrated the enhanced destabilizing capability of these composite coagulants, as shown in Fig. 7(c). Nevertheless, the zeta potential of various proportional coagulants did not reach their isoelectric points. This finding demonstrated that except for the charge neutralization, adsorption bridging and entrapment effect played important role in the coagulation treatment process.

3.3.2. Effect of OH:M on the coagulation properties and effluent pH

Fig. 8(a)–(b) presents when the dosage was  $40 \text{ mg} \cdot \text{L}^{-1}$ , the PFMS with  $n_{\text{OH:M}} = 0.32$  was the most effective sample with high  $\text{UV}_{254}$  removal efficiency of 97.61% and low turbidity of 0.36 NTU. However, when the dosage was  $9 \text{ mg} \cdot \text{L}^{-1}$ , the PFMS with OH:M = 0.18 exhibited the low  $\text{UV}_{254}$  removal efficiency of 44.04% and high turbidity of 3.2 NTU. This phenomenon can be attributed to the increased content of hydroxy complex and silicon polymer, which converted  $\text{Fe}_2(\text{SO}_4)_3$ ,  $\text{MgSO}_4$ , and  $\text{H}_2\text{SiO}_4^{2-}$  from low-molecular-weight monomer to polymer compound with high molecular weight, with the increase in the OH:M. The addition of appropriate amounts of NaOH and  $\text{NaHCO}_3$  during the preparation can further promote polymerization, and this process can be expressed by some simplified reactions (3)–(7) (the dimeric, trimeric, and polynuclear hydrolysis products of Fe and Si can also react with each other).

More importantly, given that the effluent pH of the treated water should meet the surface water treatment standards, the effluent pH at different OH:M were tested (Fig. 8(c)). When the molar ratio of OH:M was greater than 0.18, the pH of the effluent ranged between 6.5–8.5, which satisfies the specified effluent requirements for drinking water sources.

3.3.3. Effect of aging time on the particle size distribution of the PFMS coagulant and the stability of the prepared coagulant

Fig. 9 displays the colloidal particle size distribution of the

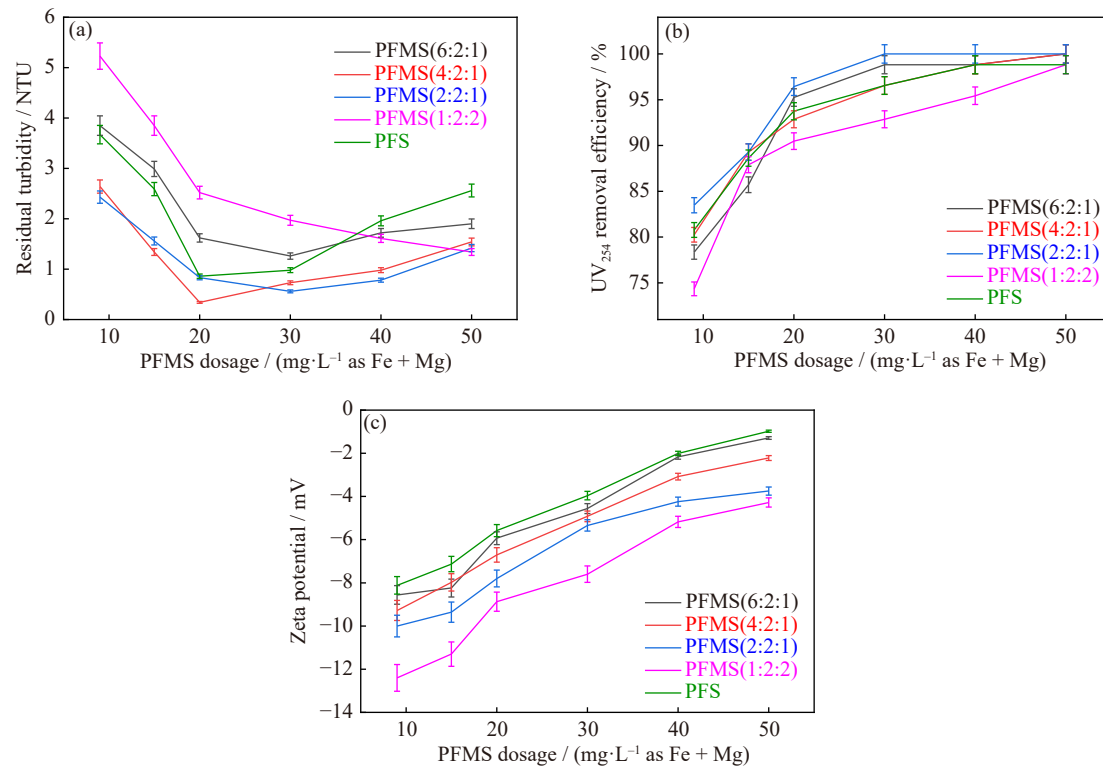


Fig. 7. Effect of Fe:Si:Mg and dosage of the PFMS on the (a) residual turbidity, (b) UV<sub>254</sub> removal efficiency, and (c) zeta potential of humic acid–kaolin synthetic surface water (experimental condition: Fe:Si:Mg = 6:2:1, 4:2:1, 2:2:1, 1:2:2; OH:M = 0.25; aging for 3 d).

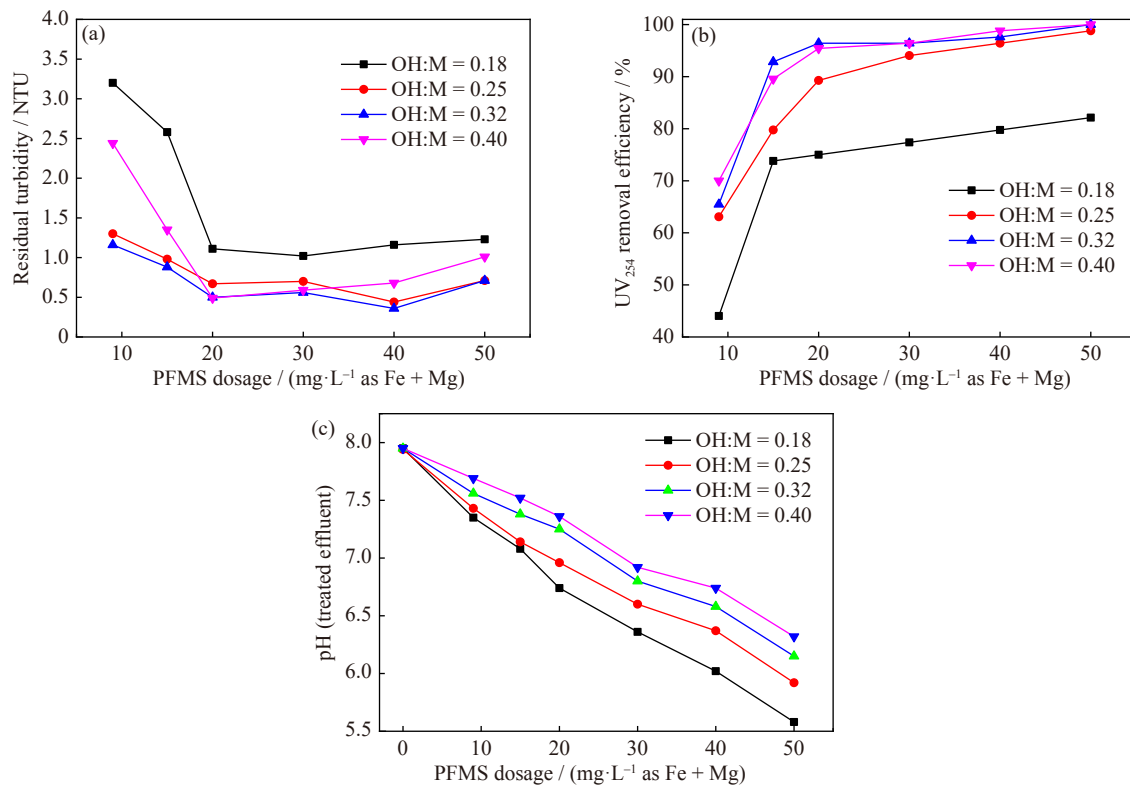


Fig. 8. Effect of OH:M on the (a) residual turbidity, (b) UV<sub>254</sub> removal efficiency, and (c) pH of the treated effluent in the treatment of humic acid–kaolin synthetic surface water (experimental condition: Fe:Si:Mg = 2:2:1; OH:M = 0.18, 0.25, 0.32, 0.40; aging for 3 d).

as-prepared PFMS at different aging time. With prolonged aging, the particle size increased gradually from 0.7–0.9, 5–7, to 100–350 nm. Furthermore, the particle size distribution changed from multipeak (0.7–0.9, 5–7, and 106–142 nm) to

single-peak distribution (100–350 nm), which suggests a more uniform distribution of particle size. It was speculated that particles size of 0.7–0.9 nm may be involved in the spontaneous hydrolysis process of Fe<sup>3+</sup>, and those size of 5–7 nm

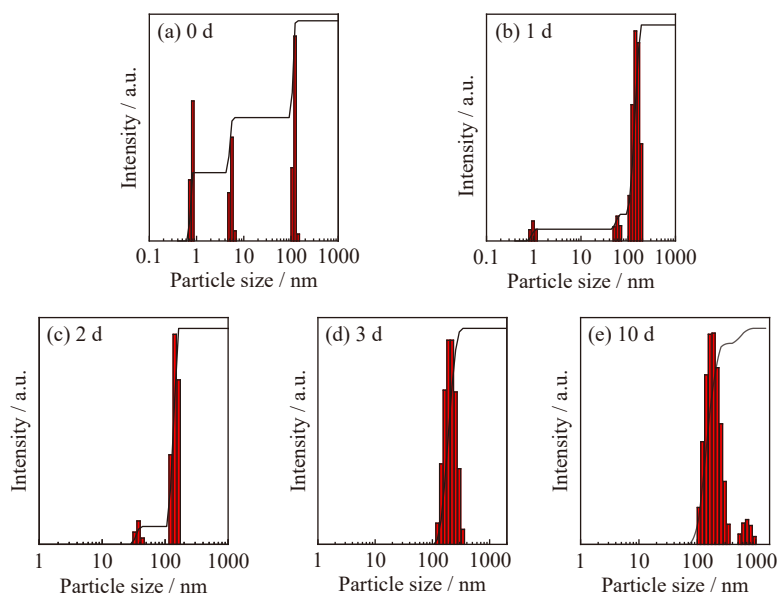


Fig. 9. Colloidal particle size distribution of PFMS aged for 0, 1, 2, 3, and 10 d.

should be assigned to the initial formation of a silicon polymer [51]. With the extension in aging time, the hydrolytic polymerization process continued, and the oligomers gradually aggregated and grew based on the specific interactions depicted in reactions (3)–(10). As Fe–OH–SO<sub>4</sub> and Mg–OH–SO<sub>4</sub> were formed during the reaction process, the formation of Fe–Mg–Si–OH–SO<sub>4</sub> was also possible.

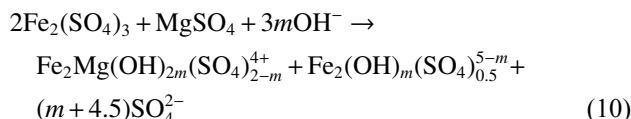
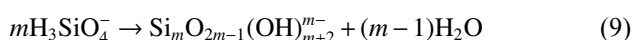
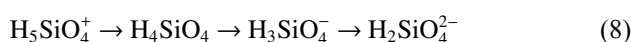
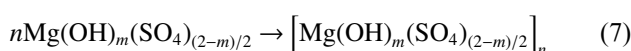
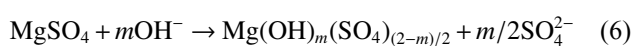
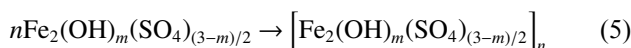
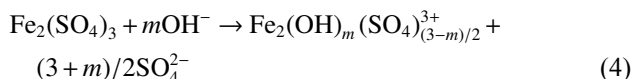
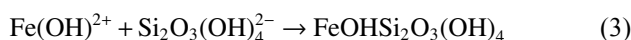
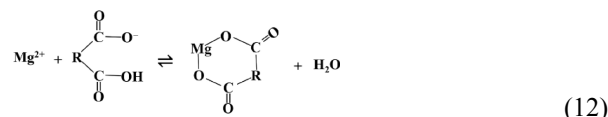
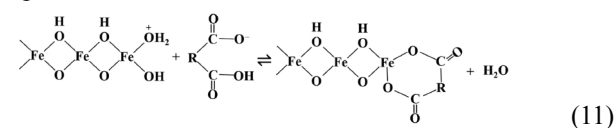


Fig. 9(d)–(e) shows that when the aging time was over 3 d, the polymerization reactions were completed as the particle size of the coagulants hardly changed. Furthermore, after retaining the PFMS for a long period (120 d), the coagulant remained without precipitation, which is beneficial for its practical use in the treatment of humic acid–kaolin synthetic surface water.

The fair stability of the new coagulant should be ensured after placing it for a long time. Otherwise, it cannot be conductive in the actual water treatment. Hence, the stability of the as-prepared samples (Fe:Si:Mg = 2:2:1 and OH:M = 0.32) was tested at room temperature (Fig. 10). After aging for 120 d, the residual turbidity was 0.49 NTU at a dosage of

20 mg·L<sup>-1</sup>, and the UV<sub>254</sub> removal efficiency was 88.12% at a dosage of 50 mg·L<sup>-1</sup>. After aging for 120 d, the residual turbidity was independent of the increased setting time, and the residual UV<sub>254</sub> changed slightly. We speculated that the net trapping and sweeping effect of the macromolecular hydroxyl complex maintained the efficient removal of the solid suspension. However, these effects reduced the formation possibility of M–humic colloids, as depicted in reactions (11)–(12). In addition, the vacant orbital outside the nucleus of Mg<sup>2+</sup> can accept the lone-pair electrons of oxygen on the hydroxyl group surface of PS molecules, iron polymers, and iron silicate complexes [52]. Therefore, the addition of magnesium dispersed the electron cloud density of the hydroxyl group and prevented the formation process of silica gel and iron hydroxide precipitate, which improved the stability of the products.



Based on the above analysis, the optimum preparation conditions of the PFMS coagulants were as follows: Fe:Si:Mg = 2:2:1, OH:M = 0.25, and aging for 3 d. At a dosage of 30 mg·L<sup>-1</sup>, the removal efficiency for UV<sub>254</sub> and the residual turbidity were 99.81% and 0.56 NTU, respectively. In addition, the PFMS coagulant reduced the residual iron content and dispersed the hydroxyl electron cloud density in the solution, which ensured a stable removal effect within 120 d.

### 3.3.4. Effect of Fe:Si:Mg on floc strength and size analysis

The strength and size of flocs formed by composite coagulants directly determine the final precipitation separation effect on the water treatment process. In general, flocs are



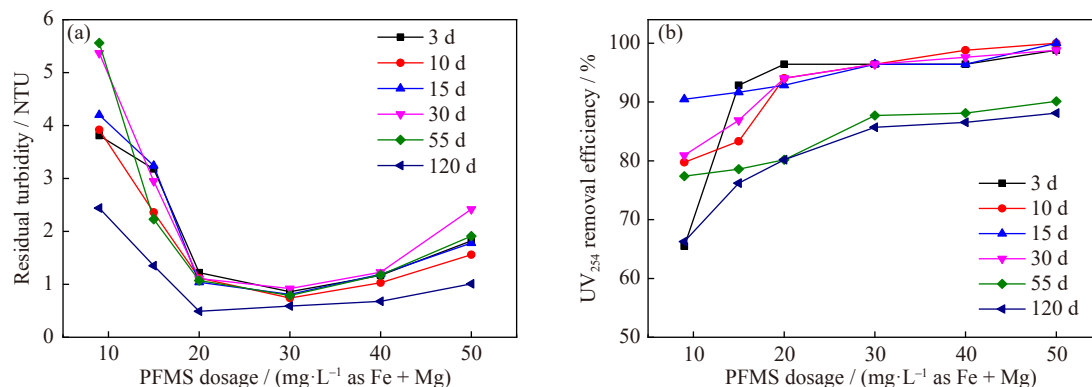


**Fig. 10.** Stability of the as-prepared PFMS coagulants in terms of (a) turbidity variation and (b) UV<sub>254</sub> removal efficiency (experimental condition: Fe:Si:Mg = 2:2:1; OH:M = 0.25; aging for 3, 10, 15, 30, 55, and 120 d).

disintegrated into small clumps under high shear forces. Thus, flocs must remain sufficiently strong to avoid this phenomenon. Otherwise, most of the microflocs (particle size less than 5  $\mu\text{m}$ ) are difficult to remove during the precipitation process, which causes water turbidity again. To discuss the strength and size of flocs, we investigated the particle size distribution characteristics of microflocs of self-made PFS (for comparison reasons) and PFMS under the same preparation conditions (Fig. 11). The agitator speed was controlled at  $2580\text{ r}\cdot\text{min}^{-1}$ , and the circulating pump speed was  $3000\text{ r}\cdot\text{min}^{-1}$  to ensure the maximum breakage of flocs.

The volume density of microflocs below 5  $\mu\text{m}$  in water samples treated with PFMS<sub>(2:2:1)</sub> was remarkably less than that of the PFS. Furthermore, the broken flocs of PFS and PFMS<sub>(2:2:1)</sub> had average particle sizes of 19.6 and 32.2  $\mu\text{m}$ , respectively. This result suggests that the introduction of  $\text{Mg}^{2+}$  increased the average size of flocs. Palmer *et al.* [53] pointed out that  $\text{Mg}^{2+}$  is conducive to pulling certain parts of individual polymer chains together via the internal crosslinking of charge neutralization and humic acid, which forces the molecule to form a compact structure and enhances floc strength. In addition, some authors [54–55] reported that divalent cations, such as  $\text{Mg}^{2+}$  and  $\text{Ca}^{2+}$ , tend to react with organic materials to form a highly dense floc structure through chemical precipitation. All these results demonstrate that the introduction of magnesium improves the strength of the floc structure.

Fig. 12 shows the coagulation mechanism of PFMS. Specifically, the inorganic suspended solids and colloidal particles in natural water mainly originated from clay minerals in the soil, and 50%–90% of organic pollutants came from humic acids, which usually possess negative charges on their

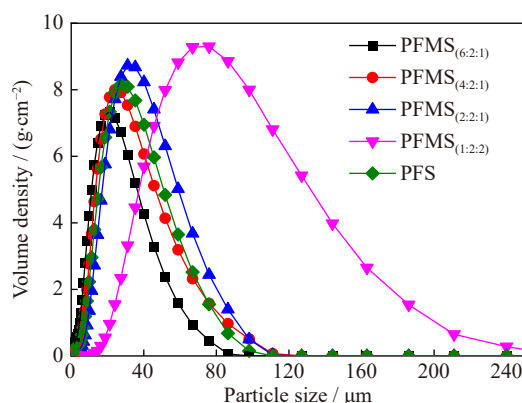


**Fig. 11.** Size distribution of broken flocs for PFS and PFMS.

surfaces. When PFMS was added to water, various hydroxyl complex ions were generated, such as Fe-based ions of  $\text{Fe}_2(\text{OH})_2^{4+}$ ,  $\text{Fe}_3(\text{OH})_4^{5+}$ , and  $\text{Fe}_6\text{O}(\text{OH})_9^{7+}$ , and Mg-based ions, including  $\text{Mg}^{2+}$  and  $\text{MgOH}^+$ , which resulted in the rapid compression of the double layer of colloidal particles in the water. Then, the negative charge on the surface was neutralized. When the electromotive potential of the colloid decreased to 0, the colloidal particles were destabilized. Moreover, in the flocculation treatment process, except for charge neutralization, adsorption bridging, net trapping, and sweeping played important roles.

In addition, during the polymerization process of silicic acid, its silicon–oxygen tetrahedral structure was interconnected and extended in space. In addition, iron interacted with the hydroxide and oxygen ions in the silicon–oxygen tetrahedral to form a new chain-like structure containing bonds, such as Si–O–Si, Fe–O–Fe, and Si–O–Fe. When the flocculant was added to the water, the destabilized particles

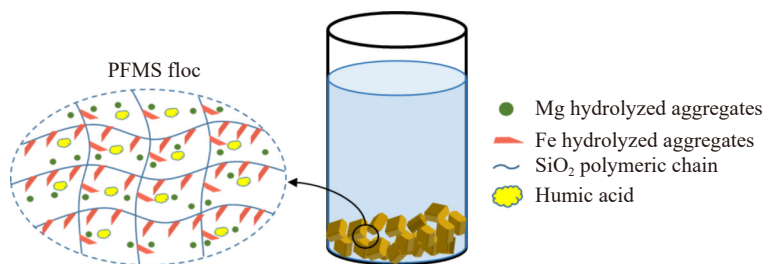
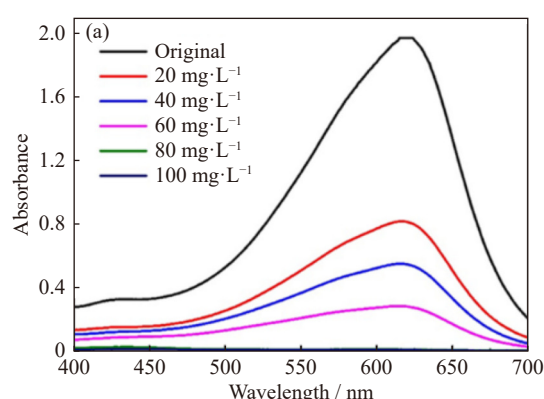


**Fig. 12.** Schematic of the coagulation mechanism of PFMS.

were adsorbed and aggregated to form large flocs due to van der Waals forces and hydrogen bonding. The PFMS obtained under the optimal preparation conditions had a relatively strong polymerization degree to form long molecular chains with strong extensibility in solutions, which greatly enhanced their bridging and coagulation capabilities. In addition, with prolonged aging, the particle size of PFMS gradually increased, and the molecular weight increased, forming a large number of multinuclear hydroxyl complexes, such as  $\text{Fe}_3(\text{OH})_4^{5+}$  and  $\text{Fe}_6\text{O}(\text{OH})_9^{7+}$ . During the precipitation process, colloidal particles in the water were involved in these hydroxide precipitates and removed.

### 3.4. Coagulation performance of optimal PFMS<sub>(2:2:1)</sub> in the treatment of reactive dye wastewater

The optimum coagulant obtained in the treatment of simulated humic acid–kaolin suspension was applied in the treatment of simulated reactive black dye wastewater to assess its



decolorization effect on industrial wastewater. Reactive azo dyes are the most problematic pollutants of textile wastewater, and they can cause mutations in humans and are toxic to aquatic life due to the aromatic amines formed by the breakdown of azo bonds [56–57]. Therefore, the coagulation performance of the optimal PFMS<sub>(2:2:1)</sub> coagulant was investigated using the most commonly used reactive black dye.

The influence of coagulant dosage and raw water pH were discussed. Based on the preliminary experiments in Fig. 13(a), the dose was set as  $80 \text{ mg} \cdot \text{L}^{-1}$ . Fig. 13(b) shows the pH played a vital role in decolorization efficiency. In the range of  $\text{pH} = 7\text{--}10$ , the decolorization rate of PFS was approximately 75%, while the decolorization rate of PMS were 15% and 45%. Notably, the addition of PFS coagulant increased the chroma of wastewater at  $\text{pH} = 11\text{--}13$ . Meanwhile, the PFMS coagulant caused the desirable decolorization at the pH range of 7–13.

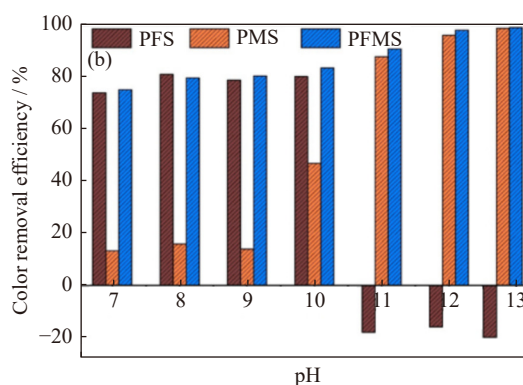


**Fig. 13.** (a) Wavelength–absorbance curve of the reactive black dye at different dosages and (b) effect of pH on the color removal efficiency of the reactive black dye (experimental condition:  $\text{Fe}:\text{Si}:\text{Mg} = 2:2:1$ ;  $\text{OH}:\text{M} = 0.25$ ; aging for 3 d).

At pH of 7–10, the decolorization mechanism of PFMS was possibly due to the dilution of the water sample and the increase in pH, which can cause the transformation of the Fe–Si polymers and production of various hydrolytic products to absorb negatively charged dye molecules. Then, an adherent bridge and catching-sweeping network formed to promote destabilized dispersions and form considerably larger flocs. Under a notably high pH,  $\text{Mg}(\text{OH})_2$  precipitates gradually formed. The solubility of  $\text{Mg}(\text{OH})_2$  is given:  $K_{\text{sp}} = [\text{Mg}^{2+}][\text{OH}^-]$ , where  $K_{\text{sp}}$  is the dissociation constant of hydroxide [25]. The formed  $\text{Mg}(\text{OH})_2$  precipitate provided a large adsorptive surface area and a positive electrostatic surface charge. The anionic groups in the dye molecule, such as  $-\text{SO}_3\text{H}$ ,  $-\text{COOH}$ ,  $-\text{OH}$ , and  $-\text{NH}_2$ , were easily used as adsorption points on the  $\text{Mg}(\text{OH})_2$  surface, and their positive electrostatic surface charge enabled them to act as powerful and efficient coagulants without other byproducts or single molecules. This finding means that PFMS removed the dye molecules by adsorption, and these molecules can be identified by the unchanged waveform of the visible spectrum and the position of the maximum absorption peak before and after coagulant addition (Fig. 12). In addition, the actual wastes collected from textile and dyestuff plants usually have a pH

of approximately 12.0, and some common coagulants cannot be used to treat such high-alkalinity wastes [34]. However, the PFMS coagulant greatly combines the advantages of magnesium and iron salts to compensate for the mentioned deficiencies.

Based on the above discussions, the as-prepared PFMS with high coagulation properties were obtained at the molar ratio of  $\text{Fe}:\text{Si}:\text{Mg} = 2:2:1$  and  $\text{OH}:\text{M} = 0.32$ .

## 4. Conclusions

The PFMS coagulants were successfully synthesized and applied to humic acid–kaolin synthetic surface water and reactive black dye wastewater. The molar ratio of  $\text{Fe}:\text{Si}:\text{Mg}$  and  $\text{OH}:\text{M}$  had remarkable effect on the microstructure and coagulation properties of the as-obtained PFMS. Under the optimum values of  $\text{Fe}:\text{Si}:\text{Mg} = 2:2:1$  and  $\text{OH}:\text{M} = 0.32$ , the as-synthesized PFMS possessed an excellent coagulation performance. The removal efficiency of  $\text{UV}_{254}$  was as high as 99.81%, and the turbidity of the surface water reached a low value of 0.56 NTU. After 120 d, the PFMS remained stable and showed remarkable coagulation properties. During the coagulation treatment process, charge neutralization, adsorp-

tion bridging, and entrapment effects played equally important roles. Furthermore, PFMS exhibited a high decolorization efficiency of 98.87% at pH = 12, indicating the good performance in the treatment of reactive dye wastewater. Compared with PFS and PMS, the PFMS coagulant enhanced the decolorization efficiency over a wide pH range by combining the advantages of PS, magnesium, and iron salts.

## Acknowledgements

This work was supported by the National Natural Science Foundation of China (No. U1810205).

## Conflict of Interest

The authors declare no potential conflict of interest.

## References

- [1] G.C. Zhu, H.L. Zheng, Z. Zhang, T. Tshukudu, P. Zhang, and X.Y. Xiang, Characterization and coagulation–flocculation behavior of polymeric aluminum ferric sulfate (PAFS), *Chem. Eng. J.*, 178(2011), p. 50.
- [2] A.K. Tolkou and A. Zouboulis, Synthesis and characterization of a novel composite pre polymerized coagulant for water and wastewater treatment, *Int. J. Environ. Eng.*, 2(2015), No. 2, p. 154.
- [3] Q.N. Ho, M. Fettweis, K.L. Spencer, and B.J. Lee, Flocculation with heterogeneous composition in water environments: A review, *Water Res.*, 213(2022), art. No. 118147.
- [4] C.L. Zhao, J.Y. Zhou, Y. Yan, et al., Application of coagulation/flocculation in oily wastewater treatment: A review, *Sci. Total Environ.*, 765(2021), art. No. 142795.
- [5] X.W. Liu, Q.K. Zhou, K.X. Li, P. Chen, M.M. Ye, and L.L. Wang, Applying permanganate/bisulfite (PM/BS) pre-oxidation enhanced coagulation to control fouling of ultrafiltration membrane in drinking waterworks, *J. Water Process. Eng.*, 52(2023), art. No. 103486.
- [6] L.H. Zhang, X.L. Liu, M.S. Zhang, T.Z. Wang, H. Tang, and Y.P. Jia, The effect of pH/PAC on the coagulation of anionic surfactant wastewater generated in the cosmetic production, *J. Environ. Chem. Eng.*, 11(2023), No. 2, art. No. 109312.
- [7] Y. Rakhila, A. Elmchaouri, A. Mestari, S. Korili, M. Abouri, and A. Gil, Adsorption recovery of Ag(I) and Au(III) from an electronics industry wastewater on a clay mineral composite, *Int. J. Miner. Metall. Mater.*, 26(2019), No. 6, p. 673.
- [8] J.S. Yuan, Y. Zhang, X.Y. Zhang, L. Zhao, H.L. Shen, and S.G. Zhang, Template-free synthesis of core–shell  $\text{Fe}_3\text{O}_4@\text{MoS}_2$ /mesoporous  $\text{TiO}_2$  magnetic photocatalyst for wastewater treatment, *Int. J. Miner. Metall. Mater.*, 30(2023), No. 1, p. 177.
- [9] A.K. Badawi and K. Zaher, Hybrid treatment system for real textile wastewater remediation based on coagulation/flocculation, adsorption and filtration processes: Performance and economic evaluation, *J. Water Process. Eng.*, 40(2021), art. No. 101963.
- [10] M.S.S. Abujazar, S.U. Karaağaç, S.S. Abu Amr, M.Y.D. Alazaiza, and M.J. Bashir, Recent advancement in the application of hybrid coagulants in coagulation–flocculation of wastewater: A review, *J. Clean. Prod.*, 345(2022), art. No. 131133.
- [11] Y. Cheng, Q.Q. Cheng, C.J. Zhao, et al., Evaluation of efficiently removing secondary effluent organic matters (EfOM) by Al-based coagulant for wastewater recycling: A case study with an industrial-scale food-processing wastewater treatment plant, *Membranes*, 13(2023), No. 5, art. No. 510.
- [12] A. Turan, M. Kobya, C. Iskurt, E. Gengec, and A. Khataee, A techno-economical assessment of treatment by coagulation–flocculation with aluminum and iron-bases coagulants of landfill leachate membrane concentrates, *Chemosphere*, 314(2023), art. No. 137750.
- [13] S.Q. Wu, B.W. Ma, C.Z. Hu, et al., Cake layer 3D structure regulation to optimize water channels during Al-based coagulation–ultrafiltration process, *Water Res.*, 236(2023), art. No. 119941.
- [14] X.Y. Wang, C. Shi, X.D. Hao, M.C.M. van Loosdrecht, and Y.Y. Wu, Synergy of phosphate recovery from sludge-incinerated ash and coagulant production by desalinated brine, *Water Res.*, 231(2023), art. No. 119658.
- [15] B.Y. Gao, Q.Y. Yue, and H.S. Huang, The research progress of water treatment of inorganic coagulating agent, *Environ. Prot. Oil Gas Fields*, 8(1998), No. 2, p. 39.
- [16] K. Hu, Q.L. Zhao, W. Chen, and F. Tang, Preparation of an aluminum and iron-based coagulant from fly ash for industrial wastewater treatment, *Clean Soil Air Water*, 45(2017), No. 9, art. No. 1600437.
- [17] G.C. Zhu, C. Wang, X.B. Liu, et al., Preparation and characterization of polymeric phosphate–aluminum sulphate for source water treatment, *Water Supply*, 16(2016), No. 4, p. 1138.
- [18] W. Chen, H.L. Zheng, H.K. Teng, et al., Enhanced coagulation–flocculation performance of iron-based coagulants: Effects of  $\text{PO}_4^{3-}$  and  $\text{SiO}_3^{2-}$  modifiers, *PLoS One*, 10(2015), No. 9, art. No. e0137116.
- [19] N. Al Otaibi, E. Bakir, and E. Afkar, Efficient alum and iron supported on silica matrix as gel coagulants for advance chemical treatment of dairy product effluents, *J. Sol Gel Sci. Technol.*, 92(2019), No. 3, p. 529.
- [20] X. Liu, X.M. Li, Q. Yang, et al., Landfill leachate pretreatment by coagulation–flocculation process using iron-based coagulants: Optimization by response surface methodology, *Chem. Eng. J.*, 200–202(2012), p. 39.
- [21] T. Coradin and J. Livage, Effect of some amino acids and peptides on silicic acid polymerization, *Colloids Surf. B*, 21(2001), No. 4, p. 329.
- [22] B.Y. Gao, H.H. Hahn, and E. Hoffmann, Evaluation of aluminum–silicate polymer composite as a coagulant for water treatment, *Water Res.*, 36(2002), No. 14, p. 3573.
- [23] Y.Y. Dai and H.Q. Qiu, Speciation analysis and coagulation behavior of PFSS, *Tech. Equip. Environ. Pollut. Control*, 6(2005), No. 3, p. 61.
- [24] A.I. Zouboulis and N.D. Tzoupanos, Polyaluminium silicate chloride—A systematic study for the preparation and application of an efficient coagulant for water or wastewater treatment, *J. Hazard. Mater.*, 162(2009), No. 2–3, p. 1379.
- [25] B.H. Tan, T.T. Teng, and A.K.M. Omar, Removal of dyes and industrial dye wastes by magnesium chloride, *Water Res.*, 34(2000), No. 2, p. 597.
- [26] Y.X. Wei, A.M. Ding, L. Dong, Y.Q. Tang, F.L. Yu, and X.Z. Dong, Characterization and coagulation performance of an inorganic coagulant—poly-magnesium–silicate–chloride in treatment of simulated dyeing wastewater, *Colloids Surf. A*, 470(2015), p. 137.
- [27] A. Tolkou and A. Zouboulis, Synthesis and coagulation performance of composite poly-aluminum–ferric–silicate–chloride coagulants in water and wastewater, *Desalin. Water Treat.*, 53(2015), No. 12, p. 3309.
- [28] P.A. Moussas and A.I. Zouboulis, A study on the properties and coagulation behaviour of modified inorganic polymeric coagulant—polyferric silicate sulphate (PFSiS), *Sep. Purif. Technol.*, 63(2008), No. 2, p. 475.
- [29] K.S. Zhang and F.C. Zeng, Preparation of poly-ferric aluminum-

- um silica sulfate coagulant from industrial wastes, *J. Chem. Ind. Eng. China*, 59(2008), No. 9, p. 2361.
- [30] Y. Fu, S.L. Yu, Y.Z. Yu, L.P. Qiu, and B. Hui, Reaction mode between Si and Fe and evaluation of optimal species in poly-silicic–ferric coagulant, *J. Environ. Sci.*, 19(2007), No. 6, p. 678.
- [31] E. Doelsch, A. Masion, J. Rose, W.E.E. Stone, J.Y. Bottero, and P.M. Bertsch, Chemistry and structure of colloids obtained by hydrolysis of Fe(III) in the presence of SiO<sub>4</sub> ligands, *Colloids Surf. A*, 217(2003), No. 1-3, p. 121.
- [32] Y. Fu, S.L. Yu, and C.W. Han, Morphology and coagulation performance during preparation of poly-silicic–ferric (PSF) coagulant, *Chem. Eng. J.*, 149(2009), No. 1-3, p. 1.
- [33] Y.B. Zeng and J. Park, Characterization and coagulation performance of a novel inorganic polymer coagulant—poly-zinc–silicate–sulfate, *Colloids Surf. A*, 334(2009), No. 1-3, p. 147.
- [34] T. Sun, L.L. Liu, L.L. Wan, and Y.P. Zhang, Effect of silicon dose on preparation and coagulation performance of poly-ferric–aluminum–silicate–sulfate from oil shale ash, *Chem. Eng. J.*, 163(2010), No. 1-2, p. 48.
- [35] W. Chen, H.L. Zheng, J. Zhai, *et al.*, Characterization and coagulation–flocculation performance of a composite coagulant: Poly-ferric–aluminum–silicate–sulfate, *Desalin. Water Treat.*, 56(2015), No. 7, p. 1776.
- [36] P. Jarvis, E. Sharp, M. Pidou, R. Molinder, S.A. Parsons, and B. Jefferson, Comparison of coagulation performance and floc properties using a novel zirconium coagulant against traditional ferric and alum coagulants, *Water Res.*, 46(2012), No. 13, p. 4179.
- [37] A.J. Jafari, M. Mahrooghi, and M. Moslemzadeh, Removal of *Escherichia coli* from synthetic turbid water using titanium tetrachloride and zirconium tetrachloride as coagulants, *Desalin. Water Treat.*, 163(2019), p. 358.
- [38] Y.X. Wei, Q.Z. Ji, L. Chen, J.W. Hao, C.L. Yao, and X.Z. Dong, Preparation of an inorganic coagulant–polysilicate–magnesium for dyeing wastewater treatment: Effect of acid medium on the characterization and coagulation performance, *J. Taiwan Inst. Chem. Eng.*, 72(2017), p. 142.
- [39] Y.X. Wei, X.Z. Dong, A.M. Ding, and D. Xie, Characterization and coagulation–flocculation behavior of an inorganic polymer coagulant–poly-ferric–zinc–sulfate, *J. Taiwan Inst. Chem. Eng.*, 58(2016), p. 351.
- [40] G.C. Zhu, Q. Wang, J. Yin, *et al.*, Toward a better understanding of coagulation for dissolved organic nitrogen using polymeric zinc–iron–phosphate coagulant, *Water Res.*, 100(2016), p. 201.
- [41] Z.M. Liu, Y.M. Sang, Z.G. Tong, Q.H. Wang, and T.C. Sun, Decolourization performance and mechanism of leachate secondary effluent using poly-aluminium(III)–magnesium(II) sulphate, *Water Environ. J.*, 26(2012), No. 1, p. 85.
- [42] H.J. Jeoung, T.H. Lee, Y. Kim, *et al.*, Use of various MgO sources for high-purity Mg metal production through molten salt electrolysis and vacuum distillation, *J. Magnesium Alloys*, 11(2023), No. 2, p. 562.
- [43] B.Y. Gao, Q.Y. Yue, Y. Wang, and W.Z. Zhou, Color removal from dye-containing wastewater by magnesium chloride, *J. Environ. Manage.*, 82(2007), No. 2, p. 167.
- [44] L. Semerjian and G.M. Ayoub, High-pH–magnesium coagulation–flocculation in wastewater treatment, *Adv. Environ. Res.*, 7(2003), No. 2, p. 389.
- [45] P.A. Moussas and A.I. Zouboulis, Synthesis, characterization and coagulation behavior of a composite coagulation reagent by the combination of polyferric sulfate (PFS) and cationic polyelectrolyte, *Sep. Purif. Technol.*, 96(2012), p. 263.
- [46] R. Li, C. He, and Y.L. He, Preparation and characterization of poly-silicic-cation coagulants by synchronous-polymerization and co-polymerization, *Chem. Eng. J.*, 223(2013), p. 869.
- [47] N.D. Tzoupanos and A.I. Zouboulis, Novel inorganic–organic composite coagulants based on aluminium, *Desalin. Water Treat.*, 13(2010), No. 1-3, p. 340.
- [48] S. Mohan and R. Gandhimathi, Removal of heavy metal ions from municipal solid waste leachate using coal fly ash as an adsorbent, *J. Hazard. Mater.*, 169(2009), No. 1-3, p. 351.
- [49] X.C. Liu, Y. Zhang, J.T. Zhou, and T.C. Cao, Experimental research on the characterization and application of Mg–Fe composite flocculant, *China Environ. Sci.*, 29(2009), No. 6, p. 646.
- [50] M. Sano, A. Kamino, and S. Shinkai, Critical coagulation of Langmuir monolayers: 2D Schulze–Hardy rule, *J. Phys. Chem. B*, 104(2000), No. 44, p. 10339.
- [51] D. Wang and H. Tang, Modified inorganic polymer flocculant–PFSi: Its preparation, characterization and coagulation behavior, *Water Res.*, 35(2001), No. 14, p. 3418.
- [52] M.Y. Liao and S.J. Randtke, Predicting the removal of soluble organic contaminants by lime softening, *Water Res.*, 20(1986), No. 1, p. 27.
- [53] N.E. Palmer and R. von Wandruszka, Dynamic light scattering measurements of particle size development in aqueous humic materials, *Fresenius J. Anal. Chem.*, 371(2001), No. 7, p. 951.
- [54] L.F. Wang, D.Q. He, W. Chen, and H.Q. Yu, Probing the roles of Ca<sup>2+</sup> and Mg<sup>2+</sup> in humic acids-induced ultrafiltration membrane fouling using an integrated approach, *Water Res.*, 81(2015), p. 325.
- [55] A.R. Costa, M.N. de Pinho, and M. Elimelech, Mechanisms of colloidal natural organic matter fouling in ultrafiltration, *J. Membr. Sci.*, 281(2006), No. 1-2, p. 716.
- [56] M.S. Lucas and J.A. Peres, Decolorization of the azo dye Reactive Black 5 by Fenton and photo-Fenton oxidation, *Dyes Pigm.*, 71(2006), No. 3, p. 236.
- [57] J. Xiao, X. Fang, S.G. Yang, H. He, and C. Sun, Microwave-assisted heterogeneous catalytic oxidation of high-concentration Reactive yellow 3 with CuFe<sub>2</sub>O<sub>4</sub>/PAC, *J. Chem. Technol. Biotechnol.*, 90(2015), No. 10, p. 1861.